J Intell Manuf
DOI 10.1007/s10845-011-0602-9

Uncertainty quantifications of Pareto optima in multiobjective problems

Tzu-Chieh Hung · Kuei-Yuan Chan

Received: 25 May 2011 / Accepted: 9 November 2011

Abstract Design is a multi-objective decision-making process considering manufacturing, cost, aesthetics, usability among many other product attributes. The set of optimal solutions, the Pareto set, indicates the trade-offs between objectives. Decision-makers generally select their own optima from the Pareto set based on personal preferences or other judgements. However, uncertainties from manufacturing processes and from operating conditions will change the performances of the Pareto optima. Evaluating the impacts of uncertainties on Pareto optima requires a large amount of data and resources. Comparing multiple Pareto solutions under uncertainty are also very costly. In this work, local Pareto set approximation is integrated with uncertainty propagation technique to quantify design variations in the objective space. An optimality influence range is proposed using linear combinations of objective functions that creates a more accurate polygon objective variation subspace. A set of 'virtual samples' is then generated to form two quantifications of the objective variation subspace, namely an influence noise to indicate how a design remains optimal, and an influence range that quantifies the overall variations of a design. In most engineering practices, a Pareto optimum with a smaller influence noise and a smaller influence range is preferred. We also extend the influence noise/range concept to nonlinear Pareto set with the second-order approximation. The quadratic local Pareto approximation method in the literature is also extended in this work to solve multi-objective engineering problems with black-box functions. The usefulness of the proposed quantification method is demonstrated using a numerical example as well as using an engineering problem in structural design.

T.-C. Hung · K.-Y. Chan (✉)
Department of Mechanical Engineering, National Cheng Kung University, 1 University Rd., Tainan, Taiwan, ROC
e-mail: chanky@mail.ncku.edu.tw

Keywords Pareto set · Uncertainty propagation · Multi-objective problems · Design under uncertainty

Introduction

Engineering design is multidisciplinary across mechanics, economics, and ecology, among many other research fields. For example, the optimization of an electronic packaging problem consists of both electronic and thermal subsystems (Du and Chen 2002); the optimal design of an air flow sensor requires both structural and aerodynamics considerations (Allison et al. 2007); an appropriate aircraft modeling combines aerodynamics, structural weight, and many other performance measures (Tappeta and Renaud 1997a,b). This type of cross disciplinary considerations is a common practice in the design of various engineering products (Giassi et al. 2004; Allison et al. 2007; Li and Azarm 2008).

In this work, multiple disciplines are considered through the existence of multiple objective functions in optimization. Each discipline has its own goal to achieve. The generalized multiobjective formulation is shown in Eq. (1) with n objective functions to be minimized simultaneously. Design variables $\mathbf{x}$ have to be in the feasible domain $\mathcal{F}$. All design constraints and bounds of $\mathbf{x}$ are implicitly included in $\mathcal{F}$.

$$\begin{aligned} \min_{\mathbf{x}} \quad & \{f_1(\mathbf{x}), f_2(\mathbf{x}), \ldots, f_n(\mathbf{x})\} \\ \text{s.t.} \quad & \mathbf{x} \in \mathcal{F} \end{aligned} \tag{1}$$

The optimal decisions of Eq. (1) will likely be on the boundary of the feasible space. Small variations of these uncertainties changes the performances of these 'optimal' design resulting in undesired output variations. Assume the uncertainties in the design variables are in the forms of manufacturing tolerances that can be modeled as $\mathbf{X} = [\mathbf{x} \pm \boldsymbol{\Delta}\mathbf{x}]$,

Published online: 18 November 2011

and the multiobjective optimization with uncertainty can be modified to Eq. (2).

$$\begin{aligned} &\min_{\mathbf{X}} \{f_1(\mathbf{X}), f_2(\mathbf{X}), \ldots, f_n(\mathbf{X})\} \\ &\text{s.t.} \quad \mathbf{X} \in \mathcal{F} \end{aligned} \tag{2}$$

Different focuses have been addressed for the formulation in Eq. (2). One focuses on the feasibility of constraints under uncertainty, also referred to as risk assessment (Rachev et al. 2008). The other one studies the optimality of objectives under uncertainty. In this work, we focus more on the change of optimality in the objective space when uncertainties are present. If the feasibility of a design under uncertainty is the main concern, the proposed method can be extended to general reliability-based design optimization(RBDO) framework (Enevoldsen and Sørensen 1994). Depending on how the uncertainties are modeled, constraints can be reformulated in probabilistic forms or in the worst-case as in Hung and Chan (2011).

The design decisions will also deviate from the original optima. Quantifying the variation in the objective space is as important as selecting a Pareto optimum as the final result might not perform as expected. In fact, these uncertainty quantifications should be included in the decision-making process to ensure an optimal yet reliable outcome.

Robust design concept is another common approach when dealing with uncertainty. Most studies in robust design literature quantify the output uncertainty using mean and variance to describe the nominal objective value and the output uncertainty variation (Doltsinis and Kang 2004; Lee and Park 2001; Jung and Lee 2002). Decision-makers should find a balance between mean performance and its variance. To account for both mean and variance, a single objective problem is transformed into a bi-objective problem. With n original objectives to be considered simultaneously, understanding the trade-offs between objective performances and objective variations become a challenging task for decision-makers.

In Hung and Chan (2011), the authors developed an optimality influence range to quantify design variations in the objective space. Optimal design alternatives are compared with not only their performances in the Pareto set but also their variations in the optimality influence range. Compared to the robust design method, optimality influence range help decision-makers understand how trade-offs between multiple objectives change under uncertainty without overwhelming the decision-makers with excessive information. An influence signal-to-noise ratio was created to indicate the accordance of objective variations to the Pareto set and an influence area was calculated to quantify the variations of a design. The extensions of the optimality influence range to complex hierarchical systems were also demonstrated. However the proposed method in Hung and Chan (2011) has two major challenges yet to be resolved. The first challenge is the extension of the optimality influence range to general n number of objective functions. When the objective space has n degrees-of-freedom, the optimality influence range can exist in infinite number of forms. This is due to the fact that the original optimality influence range is created using a vector normal to the Pareto set at a design point and a vector perpendicular to it. For $n = 2$, we can use these two vectors to create a unique optimality influence range. However, for $n > 2$, additional information is needed to yield an optimality influence range without ambiguity. The second challenge is that the optimality influence range using only the first order Taylor series expansion may not be accurate enough for highly nonlinear Pareto set.

In this work we resolves both challenges of the optimality influence range in Hung and Chan (2011) such that they can readily applicable to general nonlinear problems with n objective functions. In what follows, we will discuss the details of building an optimality influence range in "Optimality influence range in objective space". The new updated optimality influence range with higher-order Pareto approximation is developed in "Generalized optimality influence range in Pareto uncertainty quantification". The proposed method is demonstrated using a structural problem in "Engineering case study", followed by the conclusions in "Conclusions".

Optimality influence range in objective space

Design alternatives on a Pareto set are preferred if a design has good tendency to remain on the Pareto set within the prescribed tolerance regions. In this research we define the optimality influence range (OIR) in Fig. 1 that quantifies the consequences of design variations on the objectives. For a Pareto point, its objective variations due to $\boldsymbol{\Delta}\mathbf{x}$ in the design space are shown with shadows representing uncertainty. The optimality influence range is a tilted rectangle that encloses all the objective variations. Although the objective variations rarely have rectangle shapes due to nonlinearity of the functions, the optimality influence range is able to capture behaviors of objective functions under uncertainty. The unit vector $\vec{s}$ is tangent to the Pareto set at the design point and $\vec{n}$ is the vector perpendicular to $\vec{s}$. Since variations along $\vec{s}$ direction tend to 'stay' on the Pareto set while along $\vec{n}$ tend to deviate from the Pareto set, we define $\vec{s}$ as signal vector and $\vec{n}$ as noise vector. The lengths $\Delta s = \vec{s} \cdot \boldsymbol{\Delta}\mathbf{f}$ and $\Delta n = \vec{n} \cdot \boldsymbol{\Delta}\mathbf{f}$ are the signal variation and the noise variation, respectively.

An important criterion to describe the variations is that differences in objective variations should be captured. In Fig. 2, two design scenarios, A and B, on the Pareto set are shown with their variations in the objective space. These two designs have different objective variations and different tendencies

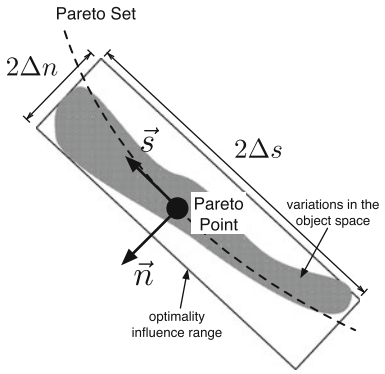

Fig. 1 Optimality influence range

to remain on the Pareto set: Scenario B has better optimality 'signal' and less 'noise' than scenario A. In a previous work (Li and Azarm 2008), these two design will end up having the same objective variation range (OVR) due to the the fact that mathematical definition of OVR is unable to describe their variations away from the Pareto set. This indicates the inability of OVR in quantifying variations in the objective space due to uncertainties in the variables/parameters. Our proposed optimality influence range extends the concept of OVR with better quantification of the variations of a Pareto point in the objective space. In this work we assume all problems have been properly scaled such that the difference between Fig. 2a, b are not the results of improper scaling.

Design selection assisted by optimality influence range

Once OIR is constructed, two important criteria can be extracted, namely the influence range for the output variations and the influence signal-to-noise ratio for the tendency to remain on the Pareto set. Area covered by the OIR, denoted as the influence range, is used to compare two Pareto design alternatives. A design with smaller influence range generally means smaller objective variation and should be preferred by designers. This criterion can simply be computed using Eq. (3) based on the OIR.

$$\text{influence range} = 2\Delta s \times 2\Delta n \tag{3}$$

The unit vector $\vec{s}$ is defined as the signal direction since variations along $\vec{s}$ tend to stay on the Pareto set while variations along the noise vector $\vec{n}$ move away from the Pareto set. With the signal and noise unit vector being defined, we introduce the influence signal-to-noise (S/N) ratio in Eq. (4) as the second criterion in selecting design alternatives.

$$\text{influence S/N ratio} = \frac{\Delta s}{\Delta n} \tag{4}$$

The influence S/N ratio differs from allowable increase/decrease in linear programming literature in that we focus on the compliance of a design to remain optimal (Neufville 1990). By doing so, we allow the design to be varied and a design considering good performance is one that remains on the Pareto set under uncertainty. The allowable increase/decrease, on the other hand, focus on the limit of uncertainty by which the optimal design starts to change. A design with a large S/N ratio tends to remain on the Pareto set: they remain optimal but at a different design point. Therefore our S/N ratio provides a better performance indication of how design behaves under uncertainty and how much attention designers should pay to improve the design.

Challenges for nonlinear Pareto set in multiple dimensions

The previous method creates an unique optimality influence range only in two-dimensional objective space. Engineering problems with more than two objective functions require additional modifications for the method to be applicable. In addition, the existing optimality influence range assumes a relatively linear Pareto set. Significant errors might exist when applying the proposed method to highly nonlinear problems that result in Pareto sets with obvious curvatures.

More specifically, when using optimality influence range for general nonlinear multiobjective decision-making, we encounter the following limitations:

- OIR is constructed via an axis that is parallel to the first order approximation of the Pareto set at a given Pareto point. When the Pareto set is curvy or when the objective variation is not along the Pareto set, OIR will over-estimate the objective variation. Figure 3 show two rectangles that encloses the same variations. As seen, the OIR in Fig. 3a is larger than that in Fig. 3b. This outcome shows that the OIR constructed by the tangent and normal vectors might not fit the objective variation. As a result, the noise in OIR is not a true measure of the objective variation. A new way to measure OIR noise is needed.
- For problems with n objective functions, the number of independent vectors required to construct OIR is n. The normal vector to a Pareto point is generally the only available vector. The rest independent vectors need to be determined judiciously. When inappropriate vectors are chosen, the OIR will not be representative and could be over conservative.

Generalized optimality influence range in Pareto uncertainty quantification

To ensure that the OIR appropriately quantifies the variation of a Pareto optimum with multiple dimensions, we develop a new method in constructing the OIR. The proposed method consists of the following steps:

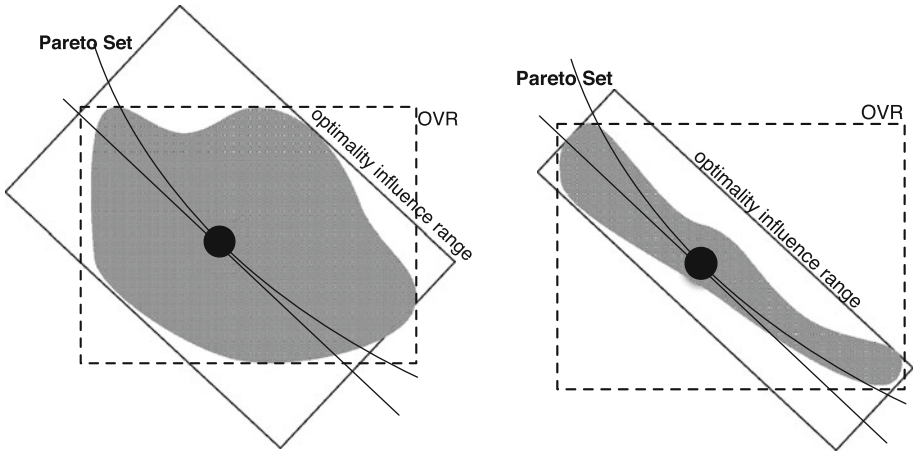

(a) Scenario A **(b)** Scenario B

Fig. 2 Comparisons between OVR in Li and Azarm (2008) and the optimality influence range. **a** Scenario A, **b** scenario B

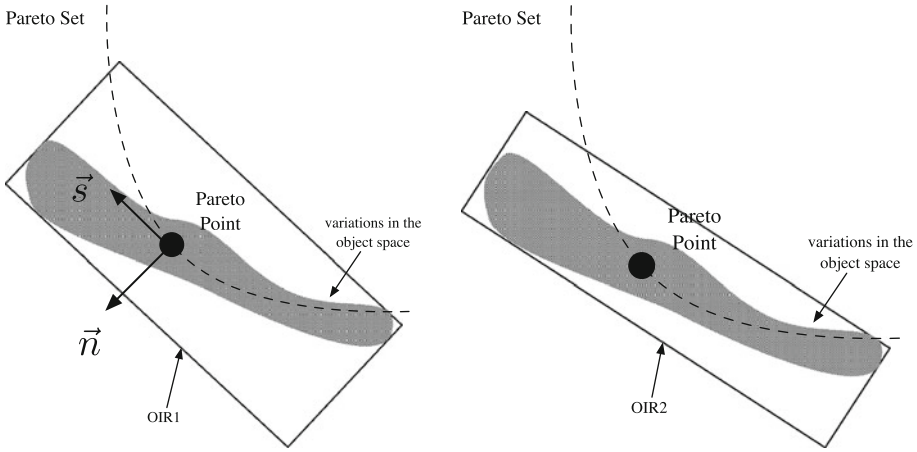

(a) Scenario A **(b)** Scenario B

Fig. 3 Impact of independent weights on OIR. **a** Scenario A, **b** scenario B

Step 0. Select a Pareto optimum.
Step 1. Generate n_w number of n-dimensional vectors to form a convex objective variation space to represent OIR.
Step 2. Generate virtual samples in OIR from Step 1.
Step 3. Calculate the overall variation via the 'range' of these virtual samples.
Step 4. Perform quadratic approximation of the Pareto set at the Pareto optimum in Step 0.
Step 5. Calculate the noise via a distance measure from virtual samples to the Pareto approximation surface.
Step 6. Make engineering decisions using these quantifications.

Steps 1–3 relate to the range of an uncertainty in objective space while steps 4 and 5 relate to how well the objective variations comply to the Pareto set. In what follows, we will use the two-dimensional problem with two objective functions in Eq. (5) for presentation purpose. Both linear and nonlinear objective functions are included. The design space is formed by variable bounds as shown. Using the bi-objective demonstration does not restrict the proposed method to the general case. The extensions to general n-dimensional objective space will be described. The variations in $\mathbf{x}$ are $\boldsymbol{\Delta}\mathbf{x} = [0.1, 0.1]^T$ in Eq. (5)

$$\begin{aligned} \min_{\mathbf{x}} \quad & f_1 = -5x_1 - 6x_2 \\ & f_2 = 3x_1^2 + 2x_1x_2 + 4x_2^2 \\ \text{s.t.} \quad & -5 \le \mathbf{x} \le 1 \\ \text{where} \quad & \mathbf{x} = [x_1, x_2]^T \end{aligned} \tag{5}$$

Step 1. Generate OIR

The original OIR rotates the variation range in the objective space with an angle tangent to the Pareto set at a given design point. When dealing with nonlinear problems, the OIR still contains unattainable areas in the objective space. In addition, the tangent plane in the original OIR can not justify an OIR with more than two objective functions.

The idea of the proposed OIR generation method is that the actual objective functions vary within a convex set of all possible sums of individual objective function with different weights. Let f^+ be the sum of the objective functions with weights $\mathbf{w}$. The weighted variation of the objective functions due to the variations $\Delta\mathbf{x}$ in the design space results in the

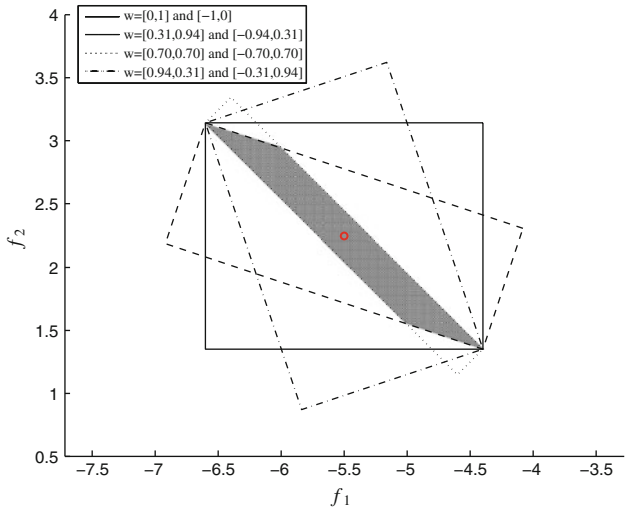

Fig. 4 Example of the convex objective variation space and the OIR

Δf^+ as in Eq. (6).

$$\Delta f^+ = \sum_{i=1}^{n} w_i \Delta f_i \tag{6}$$

In the ideal case with infinite number of different weights $\mathbf{w}$, the OIR is the intersection of the convex set formed by:

$$\text{OIR} : \bigcap_{k=1}^{\infty} \left\{ \left(\mathbf{w}_k \mathbf{f} + \Delta f_k^+\right) \left(\mathbf{w}_k \mathbf{f} - \Delta f_k^+\right) < 0 \right\}, \tag{7}$$

where k indicate the kth set of weight.

For each k, the weights should satisfy $\|\mathbf{w}_k\| = 1$. Instead of generating infinite number of weights, we create n_w number of different vectors in the n-dimensional objective space. Each set of $\{\mathbf{w}_k, \Delta f_k^+\}$ in Eq. (7) results in two parallel hyperplanes enclosing the real uncertainty variations. Figure 4 shows the convex objective variation space with eight different weights of the mathematical problem Eq. (5) at the Pareto optimum $[-5.5, 2.25]$. The final OIR is also shown as the shaded area.

Step 2. Virtual samples

The OIR constructed using Step 1 helps us refine the variation range in the objective space. Quantifiable metrics are necessary in decision-making with OIR. We have developed the influence range and the influence signal-to-noise ratio in Hung and Chan (2011) to represent the overall variation and the compliance of the variation to the Pareto set, respectively. Since a new OIR is defined and the direct implementations of the methods in Hung and Chan (2011) are not practical, we propose to cast virtual samples in the OIR to quantify influence range. The original influence S/N ratio has been changed to focus on the noise only since the number of independent signal directions increases from 1 to $(n-1)$.

We first generate n_s number of virtual samples from the set of $[\mathbf{f} \pm \boldsymbol{\Delta}\mathbf{f}]$ uniformly. Virtual samples that violate Eq. (7) are then filtered out. The remaining virtual samples with size n_sf will be evenly spread in the OIR. Figure 5a shows the 500 virtual samples before filtered and the remaining 80 samples after filtered are plotted in Fig. 5b using the example in Eq. (5).

These virtual samples are 'free' in the sense that their generation does not require any simulation of the original problem. They only represent the convex set of OIR in Eq. (7). Once virtual samples are available, we use these samples to obtain necessary information of the space they represent.

Step 3. Range calculation

The range of objective variations, $\mathcal{I}_\text{r}$, can be calculated using the Monte Carlo integration as shown in Eq. (8), where Δf_i is the individual objective variation of the ith objective function.

$$\mathcal{I}_\text{r} = \frac{n_\text{sf}}{n_\text{s}} \prod_{i=1}^{n} \Delta f_i \tag{8}$$

Step 4. First and second-order Pareto approximation

The original OIR quantifies how well a design remains optimal under uncertainty using a signal-to-noise ratio with the first order approximation of the Pareto set. The accuracy of the quantification can be improved if a higher order approximation is employed. This approximation does not require to be globally accurate. Therefore we adopt the local Pareto approximation techniques by Utyuzhnikov et al. in Utyuzhnikov et al. (2008). To make the paper self-contained, we brief the procedures developed in the literature as follows.

Let the true Pareto set be $\mathcal{S}$. The Taylor-series expansion of $\mathcal{S}$ at $\mathbf{f}^* = [f_1^*, f_2^*, \cdots, f_n^*]$, denoted as $\hat{\mathcal{S}}$ is:

$$\hat{\mathcal{S}} : f_n = f_n^* + \sum_{i=1}^{n-1} \frac{\partial f_n}{\partial f_i}(f_i - f_i^*) + \frac{1}{2} \sum_{j,k=1}^{n-1} \frac{\partial^2 f_n}{\partial f_j \partial f_k}(f_j - f_j^*)(f_k - f_k^*) + \text{h.o.t.} \tag{9}$$

where h.o.t. represents higher order terms, and the f_n is a function of f_1 to f_{n-1} mapping the nth objective function on the Pareto set. In other words, we can select one objective function and treat it as a dependent function of the rest of independent objectives. We use $\tilde{\mathbf{f}}$ to represent the set of independent objectives. f_n in Eq. (9) is then a function of $\tilde{\mathbf{f}}$ on the Pareto set.

Once the optimum on the Pareto $\mathbf{f}^*$ is selected as the expansion point, the values of partial derivatives $\partial f_n / \partial f_i$ and $\partial^2 f_n / \partial f_j \partial f_k$ in Eq. (9) will need to be calculated to obtain the local Pareto approximation. The Pareto set follows the direction of $\nabla \mathbf{f}$ and along the active constraints $\mathbf{g}$. Gradient projection method is used to obtain the vector of $\nabla \mathbf{f}$ projected on $\mathbf{g}$. Let $\mathbf{P}$ be the projection matrix and $\mathbf{J} = \nabla \mathbf{g}$ be

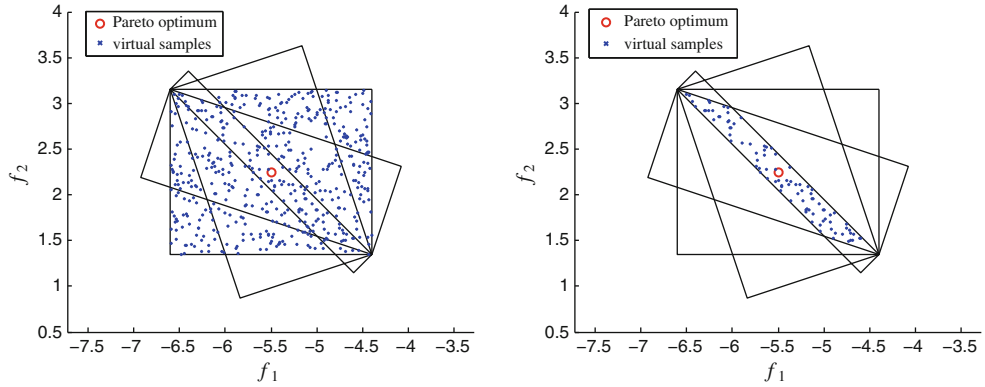

(a) The virtual samples **(b)** The filtered virtual samples

Fig. 5 Virtual samples of of Eq. (5)

the Jacobian matrix of $\mathbf{g}$. $\mathbf{P}$ can be calculated via:

$$\mathbf{P} = \mathbf{I} - \mathbf{J}\left(\mathbf{J}\mathbf{J}^T\right)^{-1}\mathbf{J}. \tag{10}$$

The projection of $\tilde{\mathbf{f}}$ onto the active constraints is denoted as $\mathbf{P}\nabla\tilde{\mathbf{f}} = (\mathbf{P}\nabla f_1, \mathbf{P}\nabla f_2, \ldots, \mathbf{P}\nabla f_{n-1})$. We then use $\mathbf{P}\nabla\tilde{\mathbf{f}}$ to represent partial derivatives of $\tilde{\mathbf{f}}$ as

$$\partial\tilde{\mathbf{f}} = (\mathbf{P}\nabla\tilde{\mathbf{f}})^T\partial\mathbf{x} \tag{11}$$

Define a matrix $\mathbf{A}$ such that

$$\mathbf{A}\partial\tilde{\mathbf{f}} = \partial\mathbf{x} \tag{12}$$

$$(\mathbf{P}\nabla\tilde{\mathbf{f}})^T\mathbf{A}\partial\tilde{\mathbf{f}} = \partial\tilde{\mathbf{f}} \tag{13}$$

After rearranging, we have

$$\mathbf{A} = \mathbf{P}\nabla\tilde{\mathbf{f}}[(\mathbf{P}\nabla\tilde{\mathbf{f}})^T\mathbf{P}\nabla\tilde{\mathbf{f}}]^{-1} = \frac{\partial\mathbf{x}}{\partial\tilde{\mathbf{f}}} \tag{14}$$

Let the ith column of $\mathbf{A}$, $\mathbf{A}_i$, be $\partial\mathbf{x}/\partial f_i$, the partial derivatives of the dependent objective function f_n with respect to the independent objective f_i as required in Eq. (9) can then be calculated via:

$$\frac{\partial f_n}{\partial f_i} = \mathbf{A}_i^T\nabla f_n \tag{15}$$

and

$$\frac{\partial^2 f_n}{\partial f_j \partial f_k} = \mathbf{A}_j^T\nabla\left(\mathbf{A}_k^T\nabla f_n\right). \tag{16}$$

Figure 6 shows the first and the second order Pareto approximation results compared with the original Pareto set. The design point is at $[-5.5, 2.25]$. As can be see including the quadratic terms improves the approximation. When functions are highly nonlinear, the differences between the linear and the quadratic approximations will be more clear.

Step 5. Noise calculation

The local Pareto approximation and the virtual samples enables the quantification of noise of a Pareto optimum. We define the noise $\mathcal{I}_\mathrm{n}$ as the deviation of the objective variations away from the Pareto. Therefore the shortest distance between the Pareto approximation surface and the virtual samples are summed up in Eq. (17) as the noise measure in this work.

$$\mathcal{I}_\mathrm{n} = \sqrt{\frac{1}{n_\mathrm{sf}}\sum_{k=1}^{n_\mathrm{sf}}\left[d\left(P_{\mathrm{f}k}, \hat{\mathcal{S}}\right)\right]^2} \tag{17}$$

where $d(P, \hat{\mathcal{S}})$ is calculated via the optimization process in Eq. (18). Although Eq. (18) needs to be calculated as many times as the number of virtual samples, it is a simple mathematical calculation that does not involve complex simulations. Both objective functions and the constraints in Eq. (18) are in at most quadratic forms, therefore the computation cost added with Eq. (18) is negligible.

$$\begin{aligned} d(P, \hat{\mathcal{S}}) : \min_{\mathbf{f}} \; & \|\mathbf{f} - P\|_2 \\ \text{s.t.} \; & \hat{\mathcal{S}}(\mathbf{f}) = 0 \end{aligned} \tag{18}$$

Step 6. Decision-making

From the Steps 0–5, we can obtain two uncertainty quantifications $\mathcal{I}_\mathrm{r}$ and $\mathcal{I}_\mathrm{n}$. Decision-makers can then use these metrics along with other performances such as the objective function values to select an optimum from the Pareto set. With uncertainty quantification, the optimal selection will not only have an ideal performances but also ensure the ideal performances are within acceptable ranges under manufacturing uncertainties. Three optimal designs are selected from the Pareto set of Eq. (5) as shown in Fig. 7. The design values, the objective function values, the objective variations as in OVR, the influence range, and the influence noise of the optima are listed in Table 1. If the variation in the objective space is the main concern, the design C with the smallest influence range and the influence noise should be selected. These values can be taken into account in a more comprehensive decision-making with f_1 and f_2.

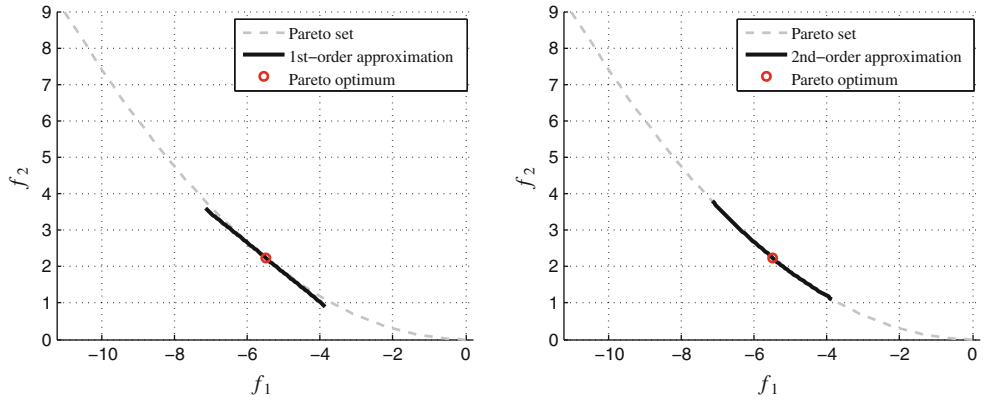

(a) The 1st-order approximation **(b)** The 2nd-order approximation

Fig. 6 Pareto approximation of Eq. (5)

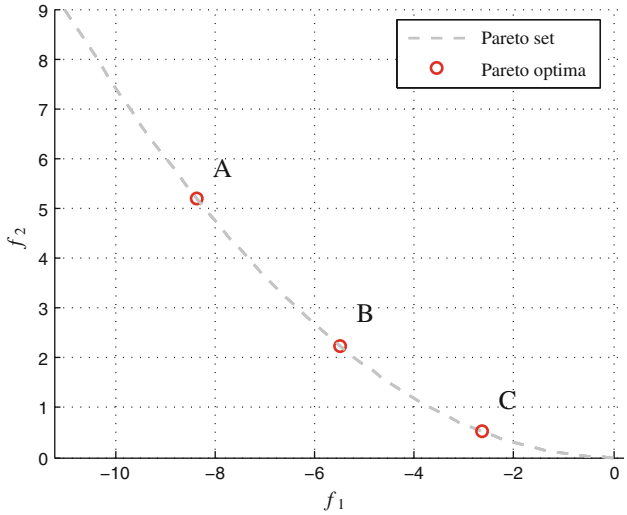

Fig. 7 Pareto points

Table 2 compares the influence range with OVR at three designs. As seen with different number of weights (8 for $\mathbf{w}^{(8)}$ and 38 for $\mathbf{w}^{(38)}$), the influence range will be different. The OVR with individual objective variation often leads to misunderstanding of the actual objective variations. If we compare the influence noise with the first and the second order approximations ($\mathcal{I}_{\mathrm{n}}^1$ and $\mathcal{I}_{\mathrm{n}}^2$). We see that the first order approximation seems to yield better results compared to 10^4 Monte Carlo simulation of the design variants. This is in fact true when a relatively linear Pareto set with a symmetric tolerance are encountered. We will show the case with nonlinear Pareto set and asymmetric tolerances in the engineering example to show the advantages of employing the second-order Pareto approximation.

Engineering case study

The three-bar structural problem as shown in Fig. 8 is studied. The ends of all bar members are pin joints. The cross-section of the bars are a_1, a_2, and a_3 with their length being l_1, l_2, and l_3, respectively. A horizontal force $F_1 = 10^5$ psi and a force $F_2 = 10^6$ psi directly downward are applied on the point P. The point P is determined by the distance b between the fixed point of bar 1 and 2. All dimensions are shown in the figure. The engineering design problem as adopted from Mattson and Messac (2005) uses the cross-section areas of all bar members and the distance b as design variables at initial point $\mathbf{x}_0 = [1, 1, 1, 720]$ with constraints on geometric layout and stress requirements. Three objective functions are optimized simultaneously, namely the structural volume, the nodal displacement at the point P, and the fundamental frequency. Cross-section areas are constrained between 0.8 and 3.0 inch square due to materials available. b is limited within 0.5–1.5 L with $L = 720$ inches. Stress constraints require that the maximal stress of each members, denoted as σ_i, can not exceed the material strength $\sigma_{\max} = 5.5 \times 10^5$ psi. Eq. (19) shows the overall problem formulation. All bar members are of the same material with Young's modulus $E = 2.9 \times 10^7$

Table 1 Comparisons of three Pareto optima

	$\mathbf{x}^*$	$\mathbf{f}^*$	$\boldsymbol{\Delta}\mathbf{f}$(OVR)	$\mathcal{I}_{\mathrm{r}}$	$\mathcal{I}_{\mathrm{n}}$
Design A	[0.79, 0.73]	[−8.36, 5.19]	[1.10, 1.37]	1.08	0.12
Design B	[0.52, 0.48]	[−5.50, 2.25]	[1.10, 0.90]	0.66	0.09
Design C	[0.25, 0.23]	[−2.64, 0.52]	[1.10, 0.43]	0.27	0.05

Table 2 Comparisons with OVR and Monte Carlo results

	$\mathcal{I}_r$	OVR	$\mathcal{I}_n^1$	$\mathcal{I}_n^2$	$\mathcal{I}_n^{MCS}$
Design A					
$\mathbf{w}^{(8)}$	1.0231	1.5037	0.1194	0.1207	0.0078
$\mathbf{w}^{(38)}$	0.0920		0.0109	0.0243	0.0080
Design B					
$\mathbf{w}^{(8)}$	0.6569	0.9893	0.0923	0.0956	0.0100
$\mathbf{w}^{(38)}$	0.0016		0.0002	0.0228	0.0100
Design C					
$\mathbf{w}^{(8)}$	0.2672	0.4748	0.0443	0.0530	0.0115
$\mathbf{w}^{(38)}$	0.1134		0.0187	0.0286	0.0118

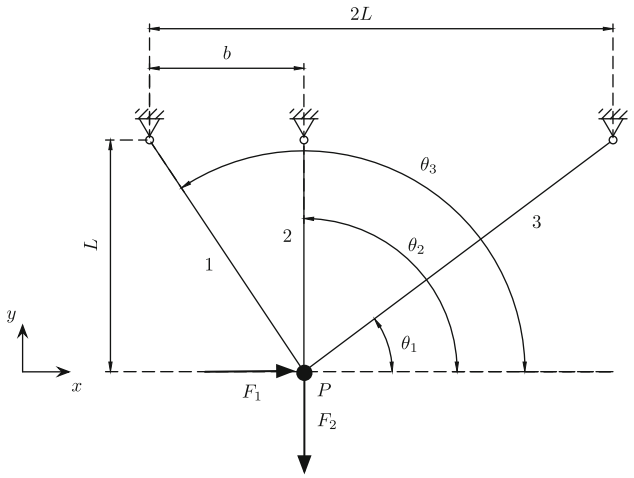

Fig. 8 Truss design example

psi and density $\rho = 7.324 \times 10^{-4}$ lbs^2/in^4.

$$\begin{aligned} \min_{\mathbf{a},b} \quad & \{f_1(\mathbf{a}, b),\ f_2(\mathbf{a}, b),\ f_3(\mathbf{a}, b)\} \\ \text{s.t.} \quad & \sigma_i \le \sigma_{\max}, \qquad i = 1, 2, 3 \\ & 0.8 \le a_i \le 3, \qquad i = 1, 2, 3 \\ & 0.5L \le b \le 1.5L \end{aligned} \tag{19}$$

The first objective function, the overall structural volume, is expressed as

$$f_1(\mathbf{a}, b) = \sum_{i=1}^{3} a_i l_i. \tag{20}$$

Finite element method is required to construct the objective functions f_2 and f_3. The reduced stiffness matrix $\mathbf{K}$ and the reduced mass matrix $\mathbf{M}$ of the truss structure are:

$$\mathbf{K} = \sum_{i=1}^{3} \frac{E a_i}{l_i} \begin{bmatrix} \cos^2\theta_i & \cos\theta_i \sin\theta_i \\ \cos\theta_i \sin\theta_i & \cos^2\theta_i \end{bmatrix} \tag{21}$$

and

$$\mathbf{M} = \sum_{i=1}^{3} \frac{\rho a_i l_i}{6} \begin{bmatrix} 2 & 0 \\ 0 & 2 \end{bmatrix}, \tag{22}$$

respectively where θ_i is the angle between the bar member i and the x-axis as shown in Fig. 8. Assuming all bars are two-force members and ignore the impact of the weight of bars, the displacement of P in x and in y direction, denoted as $\mathbf{Q} = [Q_x, Q_y]^T$, due to the external loading $\mathbf{F} = [F_1, F_2]^T$, the displacement $\mathbf{Q}$ can be obtained using Eq. (23).

$$\mathbf{KQ} = \mathbf{F} \tag{23}$$

The second objective function, the overall nodal displacement, can then be calculated via:

$$f_2(\mathbf{a}, b) = \sqrt{Q_x^2 + Q_y^2} \tag{24}$$

The maximal stress required in the constraint to prevent failure can be calculated using

$$\sigma_i = \frac{E}{l_i}(Q_x \cos\theta_i + Q_y \sin\theta_i). \tag{25}$$

The third objective function, the fundamental frequency, first uses the eigenvalue(s) of the free vibration equation in

$$\mathbf{KU} = \lambda \mathbf{MU}. \tag{26}$$

to get the frequency $\omega = \lambda^{1/2}$. The corresponding eigenvector $\mathbf{U}$ is the mode shape. The objective function f_3 is to maximize the minimal fundamental frequency as in Eq. (27).

$$f_3(\mathbf{a}, b) = -\frac{\omega_{\min}}{2\pi} \tag{27}$$

Three Pareto optima are selected as shown in Table 3. As can be seen in Fig. 9a, the second-order Pareto approximations of all three designs are reasonably accurate. With variations from design variables being 5% of initial point, $\boldsymbol{\Delta}\mathbf{x}^{\pm 5\%} = [\pm 0.05, \pm 0.05, \pm 0.05, \pm 36]^T$. The virtual samples in the objective space are compared with the propagated Monte Carlo samples from the design space to the objective space. For a three-dimensional space, different views should be provided to avoid any misleading. Therefore in this example we select design B and show the accuracy comparisons using different view angles in Fig. 9b–d. The influence range $\mathcal{I}_r$ and the influence noise $\mathcal{I}_n$ for three design are also listed in Table 3. From the comparisons, we can see that design C

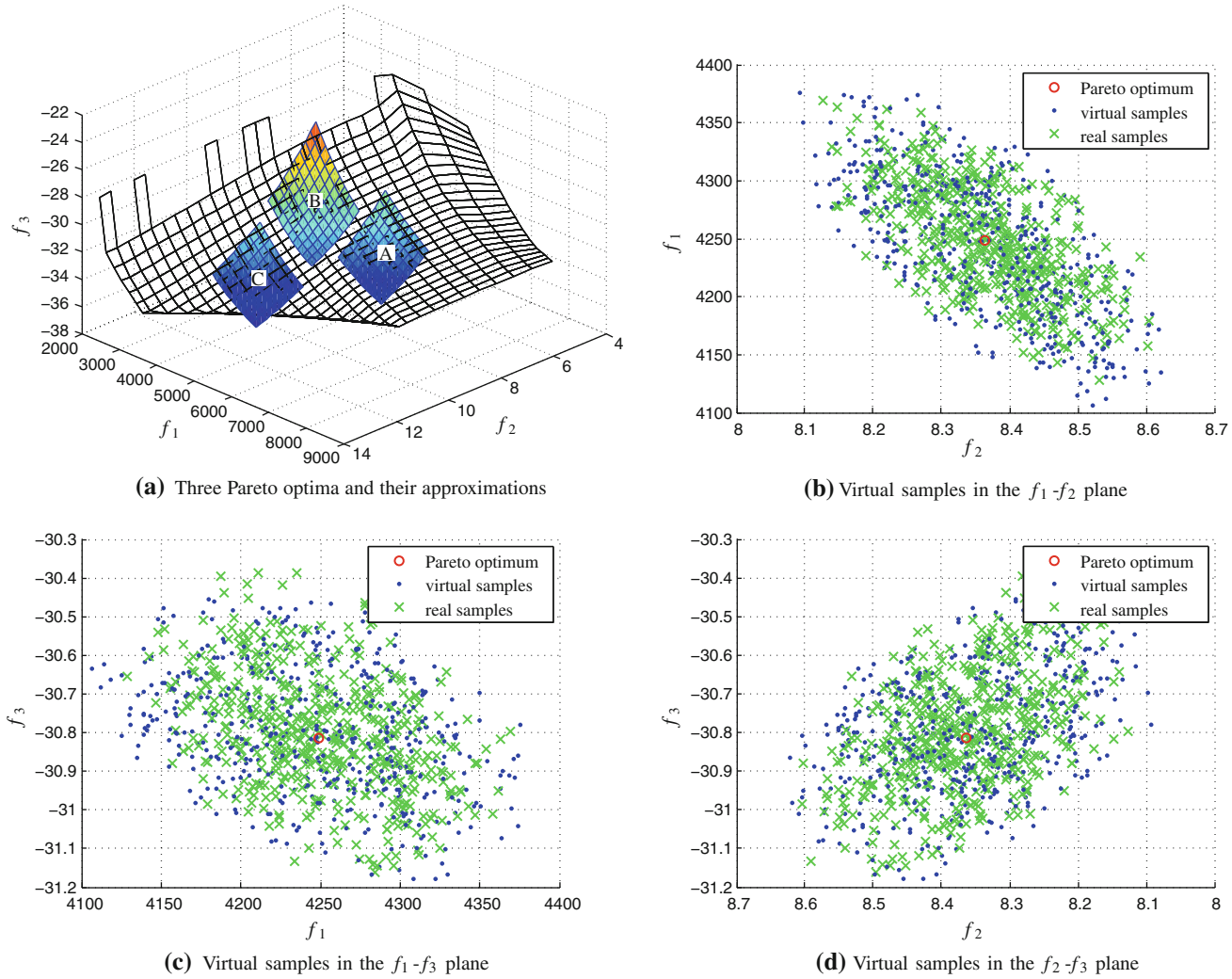

(a) Three Pareto optima and their approximations

(b) Virtual samples in the f_1-f_2 plane

(c) Virtual samples in the f_1-f_3 plane

(d) Virtual samples in the f_2-f_3 plane

Fig. 9 OIR of three Pareto design with symmetric uncertainties

Table 3 Three Pareto optimal anchor design

	$\mathbf{x}^*$	$\mathbf{f}^*$	$\boldsymbol{\Delta}\mathbf{f}$	$\mathcal{I}_r$	$\mathcal{I}_n$
Design A	2.2589	7.6131	0.0574	3.8421	0.0139
	1.7752	5, 577.7682	145.1157		
	1.9674	−33.3364	1.0720		
	700.1611				
Design B	1.5898	8.3634	0.1170	3.9782	0.0127
	1.9728	4, 248.8346	146.7401		
	1.1978	−30.8129	1.0922		
	679.7170				
Design C	1.8132	10.6143	0.0808	8.0282	0.0208
	1.1256	4, 330.8059	142.3440		
	1.6456	−34.2751	1.4175		
	706.1090				

Table 4 Uncertainty quantification with three different tolerance levels

	$\boldsymbol{\Delta x}$	$\mathcal{I}_r$	$\mathcal{I}_n$
Design A	$\boldsymbol{\Delta x}^{\pm 5\%}$	3.8421	0.0139
	$\boldsymbol{\Delta x}^{\pm 4\%}$	1.5476	0.0092
	$\boldsymbol{\Delta x}^{\pm 3\%}$	0.5467	0.0056
Design B	$\boldsymbol{\Delta x}^{\pm 5\%}$	3.9782	0.0127
	$\boldsymbol{\Delta x}^{\pm 4\%}$	1.8366	0.0080
	$\boldsymbol{\Delta x}^{\pm 3\%}$	0.5682	0.0047
Design C	$\boldsymbol{\Delta x}^{\pm 5\%}$	8.0282	0.0208
	$\boldsymbol{\Delta x}^{\pm 4\%}$	3.1746	0.0140
	$\boldsymbol{\Delta x}^{\pm 3\%}$	1.1514	0.0082

Table 5 Uncertainty quantifications with symmetric tolerances

	$\mathcal{I}_r$	OVR	$\mathcal{I}_n^1$	$\mathcal{I}_n^2$	$\mathcal{I}_n^{MCS}$
Design A	3.8421	71.4277	0.0139	0.0139	0.0108
Design B	3.9782	149.9726	0.0120	0.0127	0.0093
Design C	8.0282	130.3521	0.0206	0.0208	0.0166

Table 6 Uncertainty quantifications with asymmetric tolerances

	$\mathcal{I}_r$	OVR	$\mathcal{I}_n^1$	$\mathcal{I}_n^2$	$\mathcal{I}_n^{MCS}$
Design A	7.4873	54.5526	0.0620	0.0571	0.0406
Design B	7.6627	129.2317	0.0594	0.0500	0.0314
Design C	15.3311	112.0077	0.0995	0.0894	0.0619

has the largest variation range and the largest noise measure. That means if the Pareto design C is chosen by one designer, s/he would expect a higher impact compared to other design outcomes. Between design A and design B, A has less noise and B has better variation range. The choice between A and B has to yet to be determined by the designers with their own preferences.

Manufacturing tolerances affect the output uncertainty variation. In this case, three different tolerance levels at 3%, 4%, and 5% of the initial point are applied to the three design alternatives. The influence ranges and the influence noises are listed in Table 4. Form the comparison, we can see that the influence range and the influence noise are reduced significantly in the three design alternatives when the tolerances reduce. That means if the tolerance cost are acceptable, the designs with $\boldsymbol{\Delta x}^{\pm 3\%}$ should be a better choice for decision-makers.

Table 5 list the range and noise calculation compared with baseline using 1000 Monte Carlo design variants. As can be seen $\mathcal{I}_r$ is much smaller than OVR due to the rotation of axis. This differences not just numerically, it also affects the decision-making. For example design B has the largest variation using OVR but design C has the biggest $\mathcal{I}_r$. In addition, we also compare the noise calculation via the second order Pareto approximation versus via the first order approximation only. The noise levels in the OIR are $\mathcal{I}_n^1$ and $\mathcal{I}_n^2$ for the first and the second order approximations, respectively. As can be seen, the differences in noise measure between approximation methods are not significant. This is due to the fact that the Pareto set is smooth and the uncertainty is symmetric. For the same Pareto set with asymmetric, we can expect more clear distinctions.

When uncertainties are asymmetric with $\mathbf{X}=\left[\mathbf{x}-\boldsymbol{\Delta x}^{-0\%}, \mathbf{x}+\boldsymbol{\Delta x}^{+6\%}\right]$ where $\boldsymbol{\Delta x}^{-0\%} = [0, 0, 0, 0]^T$ and $\boldsymbol{\Delta x}^{+6\%} = [0.1, 0.1, 0.1, 72]^T$, Table 6 shows the three Pareto design and their quantification results in the influence ranges. As can be seen the design C has the largest influence area followed by design B and A. The differences in the influence noise using the first and the second order approximation become more clear in asymmetric case. The second order approximation result is closer to that of Monte Carlo simulations. The first order approximation also pass through the nominal point of the influence range and as a result overestimate the noise.

Conclusions

In this work we develop a systematic method to quantify uncertainty in the n-dimensional objective space. The

proposed optimality influence range extends the previous definition to cases with the number of objective functions $n > 2$. By rotating the original OIR with various weights, a much smaller convex space that contains the output variations is created. Virtual samples are generated to assist quantification of the OIR. An influence area that quantifies the ranges of the output variation and an influence noise that quantifies the compliance of the variation to the Pareto set are developed. We also extend the influence noise/range concept to nonlinear Pareto set with the second-order approximation. The quadratic local Pareto approximation method in the literature is also extended in this work to solve multi-objective engineering problems with black-box functions. These uncertainty quantification metrics can then be used in multi-objective decision-making.

Acknowledgments This work is partially supported by the National Science Council in Taiwan with Grant Number NSC99-2221-E-006-031. This support is highly acknowledged.

References

Allison, J., Kokkolaras, M., & Papalambros, P. (2007). On selecting single-level formulations for complex system design optimization. *Journal of Mechanical Design, 129*, 898.

Doltsinis, I., & Kang, Z. (2004). Robust design of structures using optimization methods. *Computer Methods in Applied Mechanics and Engineering, 193*(23-26), 2221–2237.

Du, X., & Chen, W. (2002). Efficient uncertainty analysis methods for multidisciplinary robust design. *AIAA Journal, 40*(3), 545–552.

Enevoldsen, I., & Sørensen, J. (1994). Reliability-based optimization in structural engineering. *Structural Safety, 15*(3), 169–196.

Giassi, A., Bennis, F., & Maisonneuve, J.-J. (2004). Multidisciplinary design optimisation and robust design approaches applied to concurrent design. *Structural and Multidisciplinary Optimization, 28*(5), 356–371.

Hung, T.-C., & Chan, K.-Y. (2011). Multi-objective design and tolerance allocation for single- and multi-level systems. *Journal of Intelligence Manufacturing*. doi:10.1007/s10845-011-0608-3.

Jung, D., & Lee, B. (2002). Development of a simple and efficient method for robust optimization. *International Journal for Numerical Methods in Engineering, 53*(9), 2201–2215.

Lee, K.-H., & Park, G.-J. (2001). Robust optimization considering tolerances of design variables. *Computers & Structures, 79*(1), 77–86.

Li, M., & Azarm, S. (2008). Multiobjective collaborative robust optimization with interval uncertainty and interdisciplinary uncertainty propagation. *Journal of Mechanical Design, 130*, 081402.

Mattson, C., & Messac, A. (2005). Pareto frontier based concept selection under uncertainty, with visualization. *Optimization and Engineering, 6*, 85–115.

Neufville, R. (1990). *Applied system analysis*. New York, NY: McGraw-Hill.

Rachev, S., Stoyanov, S., & Fabozzi, F. (2008). *Advanced stochastic models, risk assessment, and portfolio optimization: The ideal risk, uncertainty, and performance measures*. New York: Wiley.

Tappeta, R., & Renaud, J. (1997a). Multiobjective collaborative optimization. *Journal of Mechanical Design, 119*, 403–411.

Tappeta, R., & Renaud, J. (1997b). A comparison of equality constraint formulations for concurrent design optimization. *Concurrent Engineering, 5*(3), 253–261.

Utyuzhnikov, S., Maginot, J., & Guenov, M. (2008). Local Pareto approximation for multi-objective optimization. *Engineering Optimization, 40*(9), 821–847.